JOURNAL OF CHEMICAL & ENGINEERING DATA

Article

pubs.acs.org/jced

Salt-Forming Regions of the $Na^+,Mg^{2+}//Cl^-,SO_4^{2-}-H_2O$ System at 348.15 K in the Nonequilibrium State of Isothermal Boiling Evaporation

Huan Zhou,* Hongli Zhang, Yadong Chen, Jianbo Zhang, Shuai Zhang, and Xiaoqin Bai

Tianjin Key Laboratory of Marine Resources and Chemistry, College of Marine Science and Engineering, Tianjin University of Science and Technology, Tianjin TEDA, 300457, P. R. China

ABSTRACT: Industry evaporation processes are often operated at the compulsive nonequilibrium state at boiling temperature with a high evaporation intensity; meanwhile, the metastable phenomena for a complex salt−water system as $Na^+,Mg^{2+}//Cl^-,SO_4^{2-}-H_2O$ are still typical in this case. The salt-forming regions in this condition are thus more complex and not always following the solubility diagram. However, the data of the metastable equilibria are lacking in high temperature, and the stability of metastable equilibria in the industry process attracts special attention. Therefore, to know more about the behaviors of the salt-forming region departing from the equilibrium phase area, the experiments of determining the salt-forming region of the $Na^+,Mg^{2+}//Cl^-,SO_4^{2-}-H_2O$ system at 348 ± 0.2 K were carried out by the isothermal boiling evaporation method and with an evaporation intensity of (1.8 to 2.4) $g\cdot(L\cdot min)^{-1}$ (water). The salt-forming regions were determined where the regions of halite, thenardite, and loeweite are enlarged, and they are 1.99, 1.67, and 1.35 times bigger, respectively, than those in solubility diagram, whereas vanthoffite and kieserite regions are reduced. Furthermore, the diagram composed of all salt-forming regions shows four one-salt stable regions and a complex interlaced zone called the conditional region, which gives information about the stability of the salt-forming region in the nonequilibria state. In addition, comparing the salt-forming region and the solubility region, the conditional region given in the isothermal diagram accounts for 37.6 % of the diagram's total area, and it was definitely divided into two-, three-, or four-salt regions where the salts precipitating may be one or another or together which depend more on the nonthermodynamic conditions, such as crystal seed, evaporation intensity, mechanical effects, and so forth.

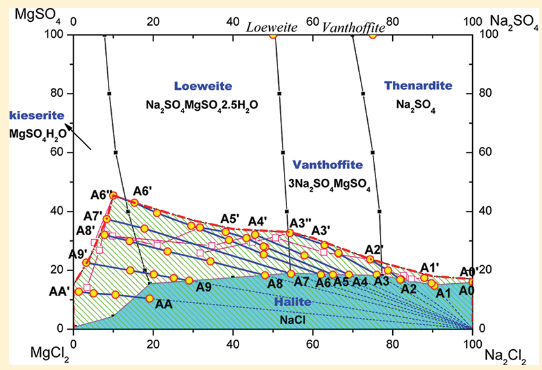

■ INTRODUCTION

Stable and metastable equilibria are typical for the complex salt−water systems, such as seawater, salt lakes, sea salt residual brine or bittern, or some industrial wastewater. Evaporation yields a crystallization sequence of various simple salts, salt hydrates, or double salts, which makes it possible to separate these salts or to recover valuable salts. Phase diagrams are thus important tools when designing fractional crystallization processes or verifying and analyzing process simulation and optimization results. However, the industry processes are usually run in the nonequilibria stable state or dynamic state where the salt-forming sequences are more complex, and even the salt-forming regions cannot be accurately predicted by a solubility diagram or metastable phase diagram. Therefore, it is still necessary to know more about the phenomena and mechanism of salt forming in a nonequilibria state.

Solubility Diagram. Began with van't Hoff, the solubility in seawater and related systems has been studied for more than 100 years.[1] Based on the second law of thermodynamics and phase rule, the methodology of isothermal solubility equilibria to determine SLE data, graphical representation, and thermodynamic modeling of solubility equilibria in multicomponent systems had been developed and used as normative guidelines for new experiments or new processes development.

Metastable Phase Diagram. Even though the amount of available solubility data is large in literature, the seawater system is still under-exploited, due to the complexity of the system or the lack of reliable data in some solubility fields.[2] Moreover, metastable phenomena usually occurs in the seawater type or other complex systems, so that its salt precipitation sequence does not always follow the solubility diagrams. Thereby, the metastable phase diagram determined by the isothermal natural evaporation method is used to present the phase regions in the metastable equilibria, such as the so-called "solar phase diagram" of $Na^+,K^+,Mg^{2+}//Cl^-,SO_4^{2-}-H_2O$ system at 298 K (partial) by Kurnakov and Nikolaev,[3] and at (288, 298, and 305) K by Jin et al.[4−6] In recent years, more data about the metastable equilibria of sulfate, carbonate, borate, and Li^+, Mg^{2+}, or Rd^+-containing systems at ambient temperature are published by Sang et al.,[7,8] Zeng et al.,[9,10] and Deng et al.[11−13]

The metastable phenomena were also studied through crystallization kinetics with the isothermal decrease of supersaturation method[14] or on solution micromechanisms with Raman spectroscopy[15] by Balarew and Tepavitcharova.

Received: November 9, 2011
Accepted: January 25, 2012
Published: February 13, 2012

Salt-Forming Behavior in a Nonequilibrium State. Industry evaporation processes such as multieffect evaporation are often operated at the compulsive nonequilibrium stable state or dynamic state at a high evaporation intensity at boiling temperatures from (323 to 393) K. Salt-forming phenomena in that case are generally more complex, and the crystallization sequence or salt-forming regions are difficult to be accurately predicted but actually play a valuable role in the industrial process. For example, in the salt plant of Qarun Salt Lake (Egypt), the four-effect evaporation crystallizers are stably running in loeweite and kieserite solubility regions and produce the desired salt of NaCl.[16]

However, the metastable equilibrium data are lacking at high temperatures, and the stability of metastable equilibrium in the industry process attracts special attention. Therefore we attempt to investigate the behaviors of the salt-forming region departing from the solubility region in a nonequilibrium state, including the departing direction, deviation degree, stability in the industry process, mechanism, and predicting method.

In our prior work, the results of the $Na^+,Mg^{2+}//SO_4^{2-}-H_2O$ system at 373 K[17] and $K^+,Mg^{2+}//SO_4^{2-}-H_2O$ system at 348 K[18] show that (1) two salts do not coprecipitated simultaneously from the costatured solution and (2) the salt-forming regions at given temperature largely depart from those in the solubility diagram. Considering the influence of crystal seed, the maximal and minimal regions of NaCl solid-forming were determined in literature,[19] which are 2.00 and 1.56 times larger than NaCl solubility region; thus it is possible to utilize the bittern resources in high efficiency.

In this study, we continue the investigation of salt-forming behaviors in the nonequilibrium state of the quaternary system of $Na^+,Mg^{2+}//Cl^-,SO_4^{2-}-H_2O$ at 348.15 K by the experimental method of isothermal boiling evaporation and attempt to obtain the forming region for all of the related salts and to discover the features of the salt-forming region at high temperatures and at a high evaporation intensity.

■ EXPERIMENT

Chemicals and Apparatus. *Chemicals.* The chemicals used were of analytical purity grade and were recrystallized several times before use. They were all obtained from the Tianjin Kermel Chemical Reagent Ltd. $MgSO_4$ (0.990 mass fraction), NaCl (0.995 mass fraction), $MgCl_2 \cdot 6H_2O$ (0.990 mass fraction), Na_2SO_4 (0.990 mass fraction), and doubly deionized water was used to prepare the series of the synthesized solution and chemical analysis.

Apparatus. Figure 1 shows the experimental apparatus. One jacketed glass evaporating crystallizer (2 L; Chemglass) with a stirrer (Heidolph), a water vapor condenser with a water collector, a thermostatic oil heating bath (Huber, K6s-cc-NR), a chemistry diaphragm pump (vacuubrand, PC 610 NT), a pressure–temperature controller, and an online recorder system were used.

Experimental Procedure. *Methodology.* The salt-forming regions were experimentally determined by the method of the isothermal boiling evaporation, that is, following the moving tracks of the liquid and solid composition within the well-mixing mixture in the isothermal boiling evaporation process, getting or estimating the first salt homogeneous nucleation point (limit solubility) and the second salt heterogeneous nucleation point (boundary point), and then expressing the whole series of representative routine and boundary points on the solubility diagram to show the salt-forming regions and behaviors.

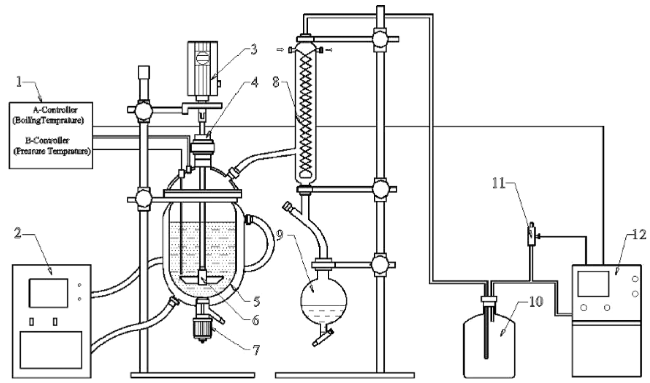

Figure 1. Experimental apparatus: 1, the controller of steam pressure and temperature; 2, thermostatic oil bath; 3, Heidolph stirrer; 4, sealed subassembly; 5, oil jacket glass evaporating crystallizer; 6, stirrer; 7, valve; 8, water vapor condenser; 9, water collector; 10, buffer bottle; 11, vacuum control valve; 12, vacuum pump.

Isothermal Boiling Evaporation. Based on the solubility data of the $Na^+,Mg^{2+}//Cl^-,SO_4^{2-}-H_2O$ system at 348.15 K,[20] 2 L of feed solution with a certain composition on the cosaturated curve (univariant) or the invariant points was prepared by the isothermal decrease of supersaturation method and was boil-evaporated at the same temperature of 348 ± 0.2 K in an oil jacket glass tank by a heating agent with a fixed temperature difference of 40 K. During the evaporation process, the boiling temperature was kept by adjusting the evaporate pressure to avoid its moving with the changes of the mixture content. The mixture was perfectly mixed by mechanical stirring in the whole process. The water vapor was condensed by 275 K cooling water, and the evaporation intensity was evaluated by the stage evaporation amount between two samples and its average volume of liquid phase.

Samples. Eight to nine solid–liquid mixture samples (25 mL for each sample) were taken through the bottom valve at the occurring point of the primary nucleation and the following points of further evaporation. Moreover, the evaporation amount was also recorded by weighing the condensed water. To keep the same composition content of the liquid and solid samples with those in the tank, the mixture samples were separated by the method of nonflash isothermal filtration, which includes three key points: (1) the isothermal filter is adopted in the vacuum filtration process, (2) to avoid the flash evaporation occurring, the absolute pressure of the vacuum filtration is not lower than that in the evaporation process, and (3) it is extremely necessary to take the vacuum filtration process in a short time which normally took (3 to 5) s in our experiments.

Chemical Analysis. The composition of the liquid phases was determined by chemical analysis. The Mg^{2+} and Cl^- ion concentrations were analyzed by volumetric methods, SO_4^{2-} by the gravimetric method, and the Na^+ ion was calculated by the subtraction method. The Mg^{2+} ion concentration was determined by the ethylenediamine tetraacetic acid (EDTA) complexometric titration at pH 10. The Cl^- ion concentration was determined by the mole method using $AgNO_3$. The composition of the SO_4^{2-} ion concentration was determined using the 0.05 M $BaCl_2$ solution. The species (see Table 1) of the solid phases were approximately evaluated with combined wet-solid-phase method, chemical analysis, or further identified with

Table 1. Related Salts of the System Na^+, Mg^{2+}//SO_4^{2-}, Cl^-−H_2O in the Equilibrium State Phase Diagram at 75 °C

salt name	chemical formula	symbol
halte	NaCl	H
thenardite	Na_2SO_4	T
loeweite	$Na_2SO_4{\cdot}MgSO_4{\cdot}2.5H_2O$	L
vanthoffite	$3Na_2SO_4{\cdot}MgSO_4$	V
kieserite	$MgSO_4{\cdot}H_2O$	K

X-ray diffraction (XRD). The ion concentrations are expressed as the Jänecke index:

$$X_i = 100z_in_i/D \qquad Y_j = 100z_jn_j/D$$
$$Z = 100n_{H_2O}/D \qquad D = \sum z_in_i = \sum z_jn_j \tag{1}$$

In eq 1, i and j are related to all cations and anions of the quaternary system. n and z are, respectively, the amount and the charge of a component. D is the mole number of all anions or cations, taking into account their charge to satisfy the electroneutrality conditions of the medium.

■ RESULTS

NaCl Solid-Forming Region. The first series representative solution (A0-A9 and AA) cosaturated with NaCl and thenardite, vanthoffite, loeweite, or kieserite, respectively, were prepared by the isothermal decrease of supersaturation and evaporated at 348 ± 0.2 K. The solid species, liquid composition, and the relevant pressure of each sample are given in Table 2. The liquid moving tracks of each representative solution are plotted in Figure 2.

During the evaporation process, only one salt of NaCl precipitates from the cosaturated solution first; meanwhile the liquid points shown in Figure 2 leave the cosaturate curve and move along with the radial line of NaCl−(A0−AA) until the second solid appears. For one typical point A6, the liquid phase (from A6 to A6″) is concentrated to 35.5 %, and NaCl precipitating

Table 2. Solid and Liquid Composition in the Isothermal Evaporation Process for the A Series Representative Points

	liquid composition (Jänecke index)			pressure			liquid composition (Jänecke index)			pressure	
no.	Na_2^{2+}	SO_4^{2-}	H_2O	KP	solid[a]	no.	Na_2^{2+}	SO_4^{2-}	H_2O	KP	solid[a]
A00	100.00	16.00	790.00	101.3		A56	31.70	34.51	632.36	26.3	H+L
A01	100.00	16.00	775.00	30.0	H[b]	A57	20.98	28.49	629.96	25.8	H+L
A02	100.00	17.00	774.00	30.0	H+T[c]	A58	8.15	32.24	504.58	22.3	H+L
A10	90.42	14.72	765.00	101.3		A60	62.00	18.50	739.10	101.3	
A11	90.42	14.72	754.00	29.5	H[b]	A61	62.00	18.50	720.00	28.8	H[b]
A12	89.70	15.56	755.00	29.8	H	A62	47.67	25.39	683.85	28.6	H
A13	87.90	17.40	757.49	29.3	H+T	A63	38.97	30.31	664.07	27.7	H
A14	84.62	17.04	762.98	29.1	H+T	A64	29.53	35.11	622.65	27.7	H
A15	82.72	18.25	781.85	29.3	H+T	A65	20.96	39.51	576.41	26.3	H
A16	78.04	19.74	731.95	29.4	H+T	A66	15.32	42.94	535.67	25.8	H
A20	82.07	16.99	772.07	101.3		A67	9.99	45.42	486.26	23.6	H+K[c]
A21	82.07	16.99	754.00	29.6	H[b]	A68	5.22	29.44	523.41	23.5	H+K
A22	81.87	16.81	755.34	29.6	H	A70	54.50	18.80	730.00	101.3	
A23	78.80	19.96	756.12	29.0	H	A71	54.50	18.80	710.00	28.0	H[b]
A24	74.31	23.69	723.48	28.9	H+T[c]	A72	17.82	34.14	553.03	27.8	H
A25	62.76	26.11	691.34	28.8	H+T	A73	8.36	37.40	541.67	21.4	H+K[c]
A26	50.68	31.06	660.96	26.9	H+V[d]	A74	6.53	26.81	501.48	19.3	H+K
A30	76.00	18.50	755.94	101.3		A75	3.40	14.12	494.26	18.7	H+K
A31	76.00	18.50	745.00	29.5	H[b]	A80	48.00	18.30	713.30	101.3	
A32	66.40	25.63	721.10	29.0	H	A81	48.00	18.30	654.00	28.0	H[b]
A33	66.37	25.85	703.09	28.6	H	A82	34.33	23.01	619.75	27.6	H
A34	62.88	28.60	674.35	28.5	H	A83	23.58	26.39	618.81	26.8	H
A35	54.23	32.68	647.11	28.4	H+V[c]	A84	14.08	29.91	570.16	25.8	H
A36	44.89	29.56	648.01	28.3	H+V	A85	7.80	32.04	489.39	25.6	H
A40	69.00	19.50	747.50	101.3		A90	29.00	16.50	662.09	101.3	
A41	69.00	19.50	742.00	29.2	H[b]	A91	29.00	16.50	637.50	27.2	H[b]
A42	57.89	25.07	728.00	27.5	H	A92	25.15	17.35	633.33	26.7	H
A43	56.03	25.90	727.25	27.2	H	A93	20.16	18.59	570.95	26.2	H
A44	45.54	32.10	651.91	27.0	H+L[c]	A94	14.25	19.96	516.95	25.4	H
A45	34.71	28.36	649.78	26.8	H+L	A95	3.24	22.57	463.34	24.9	H
A46	9.82	31.65	510.09	26.5	H+L	AA0	21.93	10.29	645.50	101.3	
A50	65.00	18.50	742.70	101.3		AA1	21.93	10.29	620.00	26.5	H[b]
A51	65.00	18.50	738.50	29.1	H[b]	AA2	19.11	10.40	574.91	24.6	H
A52	48.07	27.89	685.00	28.5	H	AA3	10.53	11.69	559.52	22.0	H
A53	47.64	28.11	681.71	27.2	H	AA4	5.06	12.16	528.34	19.8	H
A54	43.36	30.95	717.02	27.1	H+L[c]	AA5	1.38	12.72	407.40	14.8	H
A55	38.14	33.02	717.10	26.8	H+L						

[a] K, kieserite ($MgSO_4{\cdot}H_2O$); L, loeweite ($Na_2SO_4{\cdot}MgSO_4{\cdot}2.5H_2O$); V, vanthofite ($3Na_2SO_4{\cdot}MgSO_4$); T, thenardite ($Na_2SO_4$); H, halite (NaCl); T, thenardite (Na_2SO_4). [b] First salt occurring point. [c] Second salt occurring point. [d] Third salt occurring point.

dx.doi.org/10.1021/je201196q | J. Chem. Eng. Data 2012, 57, 943−951

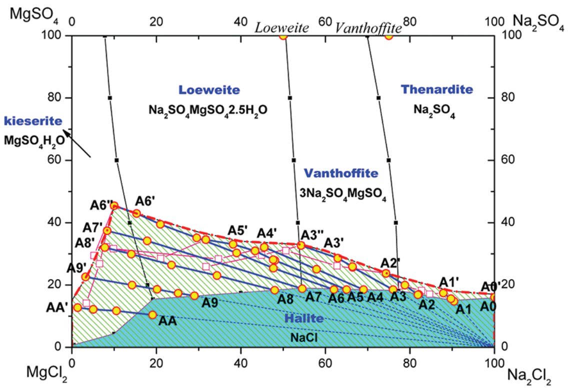

Figure 2. NaCl solid-forming region in the $Na^+,Mg^{2+}//SO_4^{2-},Cl^-{-}H_2O$ system at 348.15 K in isothermal boiling evaporation process. −■−, solubility data at 348.15 K; −○−, liquid phase tracks after the first salt (NaCl) forming; −□−, liquid phase tracks after the second salt forming; −·−, the utmost region border of NaCl solid-forming.

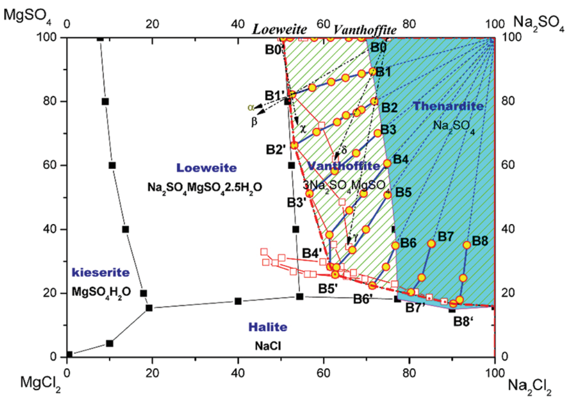

Figure 3. Na_2SO_4 solid-forming region in the $Na^+,Mg^{2+}//SO_4^{2-},Cl^-{-}H_2O$ system at 348.15 K during the isothermal boiling evaporation process. −■−, solubility data at 348.15 K; −○−, liquid phase tracks while the first salt (Na_2SO_4) is forming; −□−, liquid phase tracks while the second salt is forming; −·−, the utmost region border of Na_2SO_4 solid forming; −··−, solid−liquid vector.

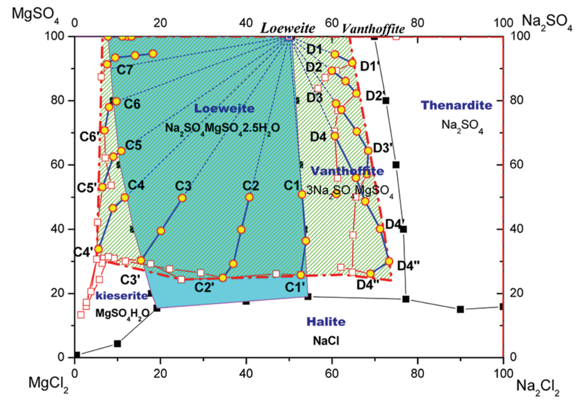

Figure 4. Loeweite solid-forming region in the $Na^+,Mg^{2+}//SO_4^{2-},Cl^-{-}H_2O$ system at 348.15 K isothermal boiling evaporation process. −■−, solubility data at 348.15 K; −○−, liquid phase tracks while loeweite is forming, −□−, liquid phase tracks while the second salt is forming; −·−, the utmost region border of loeweite forming.

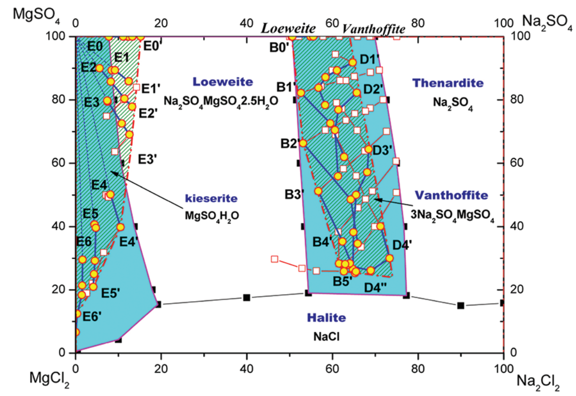

Figure 5. Vanthoffite and kieserite solid-forming region in the $Na^+,Mg^{2+}//SO_4^{2-},Cl^-{-}H_2O$ system at 348.15 K isothermal boiling evaporation process. −■−, solubility data at 348.15 K; −○−, liquid phase tracks while loeweite is forming; −□−, liquid phase tracks while the second salt is forming; −·−, the utmost region border of loeweite forming.

singly is about 93.2 % to the total amount of it in the initial feed solution. While the second salt starts to precipitate, NaCl could keep on its crystallization, and the liquid phase turns the track direction but does not reach the cosaturated curve.

The curve of the second salt occurring points of A0′−A9′−AA′ gives the boundary of the NaCl solid-forming utmost field, which enlarges the NaCl scope to the adjacent fields of thenardite a little, but vanthoffite, loeweite, and kieserite much more.

To illustrate the degree of salt-forming region departing from the solubility region, the region area on the water free diagram was calculated by the analytical tool of calculus/integrate on the OriginPro. The total area of the diagram, for example, Figure 2, is 10000 (100 × 100), and the area of NaCl forming-region is about 3012.9 which is 1.99 times bigger than the NaCl solubility region (1511.2).

Na_2SO_4 Solid-Forming Region. The second series representative solutions B0−B6 cosaturated with Na_2SO_4 and vanthoffite were prepared and evaporated at the fixed boiling temperature of 348 ± 0.2 K. In addition, the points B7 and B8 within the middle of Na_2SO_4 region were selected to determine the boundary of Na_2SO_4 and NaCl regions while Na_2SO_4 solid phase precipitated first. The experimental data are given in Table 3 and plotted in Figure 3.

Figure 3 shows the departing direction and the deviation degree of the Na_2SO_4-forming region.

(1) For the cosaturated solutions (B0−B6), the solid salt precipitating first is thenardite, and the liquid phase moves along with the radial lines of Na_2SO_4−(B0−B6) in the vanthoffite equilibria region, until it reaches a turning point where the second salt occurs, which is vanthoffite for B0−B5 and NaCl for B6. For one representative point B2, the liquid phase from B2 to B2′ is concentrated to 53.65 %, and the ratio of Na_2SO_4 single precipitating is about 74.7 % to the total amount of it in the initial feed solution.

(2) While the second solid phase occurs for the series of experiments of B0−B5 at the turning points (B0′, B1′, B2′, B3′, B4′, B5′), the liquid moving tracks change their direction but, for example, like B1′ in Figure 3, do not follow the vectors of α (thenardite), β (vanthoffite), χ (loeweite), or their combined vector. The composition of the final solid phase close to vanthoffite solid point and its XRD show that thenardite and vanthoffite exist but no loeweite. The final solid−liquid vectors (e.g., δ for B1 feed solution and γ for B2 feed solution in Figure 3) just correspond to the theoretical analysis results in the

dx.doi.org/10.1021/je201196q | J. Chem. Eng. Data 2012, 57, 943−951

Table 3. Solid and Liquid Composition in the Isothermal Evaporation Process for the B Series Representative Points

	liquid composition (Jänecke index)			pressure			liquid composition (Jänecke index)			pressure	
no.	Na_2^{2+}	SO_4^{2-}	H_2O	KP	solid[a]	no.	Na_2^{2+}	SO_4^{2-}	H_2O	KP	solid[a]
B01	69.01	100.00	725.00	101.3		B40	74.84	60.63	797.50	101.3	T
B02	69.01	100.00	580.00	39.2	T[b]	B41	74.84	60.63	727.31	35.6	T
B03	68.72	100.00	581.00	37.5	T	B42	69.30	51.21	768.83	35.7	T
B04	65.85	100.00	582.00	37.2	T	B43	65.97	45.92	725.32	36.3	T
B05	61.58	100.00	583.00	37.2	T	B44	61.32	38.31	697.47	36.9	T
B06	57.78	100.00	584.00	37.3	T	B45	61.55	28.29	687.96	33.3	T+V[c]
B07	52.14	100.00	585.00	37.3	T	B46	64.06	28.33	701.38	35.4	V
B08	50.44	100.00	586.00	36.8	T+V[c]	B50	74.91	50.77	796.20	101.3	
B09	54.90	100.00	587.00	36.8	V	B51	74.91	50.77	745.59	33.4	T[b]
B10	70.94	89.39	742.50	101.3	V	B52	69.86	39.97	758.98	33.4	T
B10	70.94	89.39	693.00	38.2		B53	66.68	33.51	725.40	32.5	T
B11	68.87	88.73	694.33	37.0	T[b]	B54	62.94	28.11	694.66	31.6	T
B12	65.11	87.43	700.00	37.0	T	B55	62.65	25.84	695.82	31.6	T+V[c]
B13	61.73	86.11	687.82	37.0	T	B56	56.24	26.02	700.24	31.8	V
B14	57.31	84.32	672.30	36.1	T	B57	52.89	26.77	676.23	31.2	V+H[d]
B15	52.62	82.20	647.13	36.1	T	B58	46.49	29.72	667.43	31.4	V+H
B16	59.51	72.62	697.78	41.9	T+V[c]	B60	76.95	35.04	790.00	101.3	
B17	62.71	61.96	715.95	44.4	V	B61	76.77	34.91	758.19	38.6	T[b]
B18	70.94	89.39	742.50	101.3	V	B62	74.54	28.26	748.01	32.1	T
B20	71.81	80.04	786.34	101.3	V	B63	71.38	22.39	715.51	35.2	T+H[c]
B21	71.81	80.04	755.00	37.5		B64	69.59	24.49	770.13	35.8	T+H
B22	68.81	77.45	833.23	36.9	T[b]	B65	57.53	25.94	695.47	38.0	T+H
B23	67.68	76.49	857.75	36.9	T	B66	48.66	29.52	664.31	38.2	T+H
B24	65.23	75.68	824.17	37.1	T	B67	46.08	32.95	712.30	38.2	T+H
B25	63.14	73.58	730.65	36.2	T	B70	85.12	35.53	854.00	101.30	
B26	58.30	70.45	708.17	35.4	T	B71	85.12	35.53	784.75	36.00	T[b]
B27	53.14	66.29	682.00	35.3	T+V[c]	B72	82.84	24.94	781.08	34.50	T
B28	64.24	48.58	746.60	34.5	V	B73	80.39	20.31	752.32	36.30	T+H[c]
B29	65.88	34.60	740.87	34.5	V	B74	76.57	22.93	739.63	36.30	T+H
B30	66.24	31.89	714.83	34.5	V	B75	66.97	26.44	702.02	38.80	T+H
B30	72.62	70.09	939.57	101.3		B76	59.77	29.81	687.22	39.10	T+H
B31	72.62	70.09	776.50	38.0	T[b]	B77	50.18	31.10	666.10	40.20	T+H
B32	72.63	70.07	725.01	35.8	T	B80	93.43	35.09	886.30	101.30	
B33	67.57	63.86	761.40	35.7	T	B81	93.43	35.09	829.44	35.10	T[b]
B34	62.56	58.26	738.26	35.8	T	B82	92.55	24.78	837.32	33.80	T
B35	56.70	51.23	709.63	35.0	T+V[c]	B83	91.78	17.96	776.15	34.30	T
B36	62.35	35.28	731.61	33.4	T	B84	90.24	16.75	769.95	36.00	T+H[c]
B37	65.28	25.33	709.56	31.7	T	B85	88.13	17.38	761.95	37.20	T+H
B38	65.45	25.79	709.34	31.7		B86	84.67	18.73	754.87	37.20	T+H
B39	63.67	27.92	692.30	31.7	T[b]	B87	81.42	20.42	749.57	37.90	T+H

[a]K, kieserite ($MgSO_4 \cdot H_2O$); L, loeweite($Na_2SO_4 \cdot MgSO_4 \cdot 2.5H_2O$); V, vanthofite ($3Na_2SO_4 \cdot MgSO_4$); T, thenardite($Na_2SO_4$); H, halite (NaCl); T, thenardite (Na_2SO_4). [b]First salt occurring point. [c]Second salt occurring point. [d]Third salt occurring point.

equilibria solubility diagram; that is, only one salt vanthoffite theoretically precipitated while evaporating the solution B1 or B2. However the actual process in the nonequilibria state takes a very different direction where the thenardite precipitates first, and while the second solid of vanthoffite starts to precipitate, the thenardite stops its precipitating and starts to dissolve.

(3) For B6−B8, while the second salt NaCl precipitates, the Na_2SO_4 could coprecipitate with NaCl, but the liquid phase cannot reach the solubility cosaturated curve.

(4) The curve of the second salt occurring points of B0′−B8′ gives the boundary of the Na_2SO_4 solid-forming region which expands to vanthoffite equilibria fields and has an total area about 3564.6 that is 1.67 times of 2131.6 for the Na_2SO_4 solubility region.

Loeweite Salt-Forming Region. The third and fourth series representative solutions of C1−C8 and D1−D4 were evaporated to the features of loeweite and vanthoffite solid forming regions. The results are showed in Table 4, Table 5, and Figure 4.

Figure 4 shows loeweite forming behavior. Loeweite precipitates first until the second salt nucleation occurs, which is NaCl for solutions C1−C3, kieserite for C4, and vanthoffite for D1−D4, respectively. However for the solutions C5−C6 cosaturated with loeweite and kieserite, the two salts could precipitate together but in different rates, so that the liquid route does not follow the cosaturated curve. For C7−C8 located in loeweite equilibria region, loeweite precipitates first, and then the liquid phase moves to the Kieserite region. We also took the points at the cosaturated curve of loeweite and vanthoffite, but the liquid moving tracks are

Table 4. Solid and Liquid Composition in the Isothermal Evaporation Process for the C Series Representative Points

	liquid composition (Jänecke index)			pressure			liquid composition (Jänecke index)			pressure	
no.	Na_2^{2+}	SO_4^{2-}	H_2O	KP	solid[a]	no.	Na_2^{2+}	SO_4^{2-}	H_2O	KP	solid[a]
C10	53.39	49.43	715.00	101.3		C44	3.81	20.58	496.45	23.2	L+K
C11	53.39	49.43	662.22	33.9	L[b]	C45	1.45	13.31	457.77	23.1	L+K+H[d]
C12	53.89	36.35	705.57	32.4	L	C50	10.89	64.36	587.50	101.3	
C13	52.70	25.69	702.05	32.0	L+H[c]	C51	10.89	64.36	479.15	27.9	L[b]
C14	47.00	26.05	684.23	37.2	L+H	C52	9.05	62.53	492.15	27.4	L
C15	24.89	24.34	681.99	37.3	L+H	C53	6.49	53.06	516.46	27.6	L+K[c]
C16	17.74	29.21	565.30	37.3	L+H	C54	5.36	42.10	529.15	26.6	L+K
C20	40.78	49.90	665.15	101.3		C55	5.15	30.64	530.57	26.6	L+K
C21	40.71	50.00	646.16	32.1	L[b]	C56	2.78	17.17	530.28	24.6	K+H[d]
C22	38.82	39.86	669.16	31.2	L	C60	9.76	79.81	562.50	101.3	
C23	36.96	29.18	648.53	31.2	L	C61	9.76	79.81	476.30	34.8	L[b]
C24	34.54	24.84	648.00	30.5	L+H[c]	C62	9.95	79.69	463.17	30.6	L
C25	29.40	26.39	647.06	29.6	L+H	C63	8.03	78.00	458.50	29.2	L+K[c]
C26	22.17	27.62	614.98	28.4	L+H	C64	6.97	70.73	494.17	29.4	L+K
C27	11.85	30.03	545.87	75.4	L+H	C65	7.14	62.18	492.26	34.5	L+K
C28	6.78	30.93	516.59	31.3	L+H	C66	8.51	53.63	557.94	37.4	K+H[d]
C29	6.41	29.43	541.75	31.1	L+H+K[d]	C70	18.21	94.64	552.30	101.3	
C30	25.08	49.68	619.17	101.3		C71	18.27	94.67	451.30	24.9	L[b]
C31	25.08	49.68	589.20	31.8	L[b]	C72	14.10	94.10	489.61	24.4	L
C32	20.11	39.50	600.28	30.4	L	C73	9.43	93.41	497.19	24.3	L
C33	15.47	30.27	583.70	28.0	L	C74	7.58	91.38	511.81	24.3	L+K[c]
C34	9.18	30.92	531.38	25.9	L+H[c]	C75	6.20	87.45	526.20	0.0	L+K
C35	7.84	31.42	506.91	29.5	L+H	C80	13.32	100.00	540.00	101.3	
C36	5.75	24.34	508.42	31.6	L+H+K[d]	C81	13.32	100.00	678.02	29.0	L[b]
C37	2.71	15.94	480.58	30.6	H+K	C82	12.44	100.00	491.60	26.0	L
C40	10.94	50.20	576.30	101.3		C83	12.36	100.00	469.98	0.0	L
C41	10.94	50.20	529.70	30.5	L[b]	C84	11.12	100.00	477.32	25.0	L+K[c]
C42	8.92	46.56	519.61	33.6	L	C85	7.77	100.00	492.00	25.4	L+K
C43	5.54	33.75	504.89	24.2	L+K[c]						

[a] K, kieserite ($MgSO_4 \cdot H_2O$); L, loeweite ($Na_2SO_4 \cdot MgSO_4 \cdot 2.5H_2O$); V, vanthofite ($3Na_2SO_4 \cdot MgSO_4$); T, thenardite ($Na_2SO_4$); H, halite (NaCl); T, thenardite (Na_2SO_4). [b] First salt occurring point. [c] Second salt occurring point. [d] Third salt occurring point.

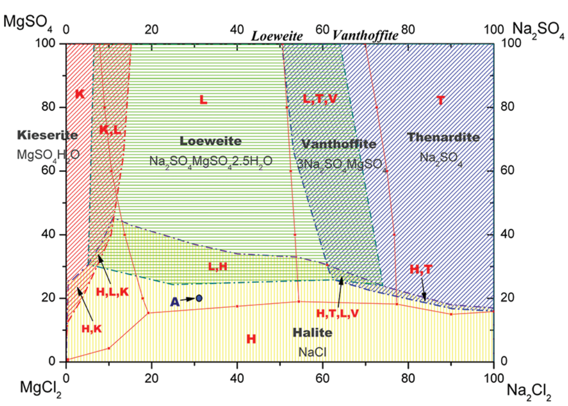

Figure 6. Isothermal salt-forming diagram of the $Na^+,Mg^{2+}//Cl^-,SO_4^{2-}-H_2O$ system at 348.15 K in a nonequilibrium state. –■–, solubility data at 348.15 K; –·–, border for the extended salt-forming region. K, L, V, T, and H denote the single salt region for kieserite, loeweite, vanthoffite, thenardite, and halite. K+L, H+T, L+H, and H+K denote that the region may be one or another or a region formed together. L+T+V, H+L+K, and H+T+L+V denote that the region may be one, two, or three salts that could be formed in different conditions.

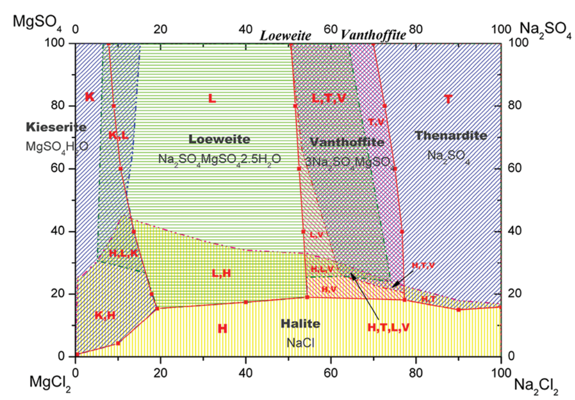

Figure 7. Isothermal phase diagram of the $Na^+,Mg^{2+}//Cl^-,SO_4^{2-}-H_2O$ system at 348.15 K between equilibrium and nonequilibrium states. –■–, solubility data at 348.15 K; –·–, border for the extended salt-forming region. K, L, V, T, and H denote the single salt region for kieserite, loeweite, vanthoffite, thenardite, and halite. K+L, H+T, L+H, and H+K denote that the region may be one or another or a region formed together. L+T+V, H+L+K, and H+T+L+V denote that the region may be one, two, or three salts that could be formed in different conditions.

more like C1 solution. So we chose D1–D4 in the middle of the vanthoffite solubility region. It is noticeable that the first salt precipitating is still loeweite.

The loeweite solid-forming region is enlarged to the kieserite and vanthoffite field but decreased by the NaCl scope. Thus, the loeweite forming region has an area of about 4667.3, which is 1.35 times bigger than 3380.6 for its solubility region.

Table 5. Solid and Liquid Composition in the Isothermal Evaporation Process for the D Series Representative Points

no.	liquid composition (Jänecke index) Na_2^{2+}	SO_4^{2-}	H_2O	pressure KP	solid[a]	no.	liquid composition (Jänecke index) Na_2^{2+}	SO_4^{2-}	H_2O	pressure KP	solid[a]
D10	60.64	94.44	716.75	101.3		D32	62.17	77.22	650.38	27.8	L
D11	60.47	94.05	585.25	30.2	L[b]	D33	65.75	70.40	695.50	28.8	L
D12	64.73	91.78	650.18	29.5	L+V[c]	D34	68.42	64.41	719.20	28.8	L
D13	61.02	89.34	692.34	31.4	V	D35	68.09	57.17	774.58	28.6	L+V[c]
D14	58.36	87.18	692.03	32.6	V	D36	65.49	50.04	744.84	30.3	V
D15	56.73	83.81	694.57	32.6	V	D37	64.89	38.16	738.39	29.9	V+L
D16	58.27	78.37	711.39	31.6	V+L[c]	D38	64.74	26.57	703.82	29.9	V+L
D20	59.93	89.35	691.00	101.3		D40	60.66	68.99	741.30	101.3	
D21	60.50	89.64	608.75	29.4	L[b]	D41	60.06	68.80	633.00	29.4	L[b]
D22	63.12	86.14	647.86	28.7	L	D42	65.57	55.96	715.27	29.5	L
D23	65.66	82.23	667.59	28.8	L+V[c]	D43	67.74	48.68	744.61	29.6	L
D24	61.39	76.95	695.46	28.9	V	D44	71.20	40.11	719.80	29.6	L
D25	60.56	70.48	713.73	29.7	V+L	D45	73.31	29.97	715.83	29.3	L+V[c]
D26	61.28	55.87	713.28	32.3	V+L	D46	68.94	26.09	700.55	30.3	L+H[d]
D30	60.92	79.14	702.00	101.3		D46	62.04	28.14	690.22	29.8	L+H
D31	60.54	79.19	643.67	28.8	L[b]						

[a]K, kieserite ($MgSO_4·H_2O$); L, loeweite ($Na_2SO_4·MgSO_4·2.5H_2O$); V, vanthofite ($3Na_2SO_4·MgSO_4$); T, thenardite (Na_2SO_4); H, halite (NaCl); T, thenardite (Na_2SO_4). [b]First salt occurring point. [c]Second salt occurring point. [d]Third salt occurring point.

(1) **Vanthoffite- and Kieserite-Forming Regions.** The vanthoffite-forming region shown in Figure 5 by combining Figures 3 and 4 is more invaded and occupied by thenardite and loeweite, respectively, and takes a narrow area about 1044.8 (accounting for 58.4 % of the equilibria region). Moreover vanthoffite is formed only after the first salt precipitated, and its homogeneous nucleation is not found in the experimental conditions.

(2) To determine the kieserite-forming region when it formed first, E0−E6 within the middle of its solubility region were chosen. The results are given in Table 6 and shown in Figure 5.

In Figure 5, the area of the kieserite one-salt region is reduced from 1188.8 in the solubility region to 945.3. It seems that the kieserite solubility region is easily occupied by NaCl. But kieserite also has the capability of occupying the loeweite equilibria region only while enough loeweite solid exists. This phenomenon will be discussed later.

■ DISCUSSION

Mechanism of Salt-Forming Region on Crystallization Kinetics. Theoretically, it is impossible that the forming-region of loeweite or kieserite is occupied by NaCl in its own solubility region when its solid phase exists at first. However, in our experimental conditions, the actual result shown in Figures 4 and 5 indicates that, although the loeweite or kieserite solid phase existd at first in its own solubility field (e.g., the points C1′, C2′, C3′, E4′, E5′, E6′), the primary nucleation of NaCl also occurs. The prior results of ref 17 and 18 show that, during the same evpaoration conditions, the different salts keep different degreed of supersaturation. In this work, we noticed that, at the same evaporation intensity, the SL mixture kept a higher degree of supersaturation for loeweite or kieserite nucleation and crystal growth but kept a lower degree for NaCl. So the solutions of C1′, C2′, C3′, and E4′, E5′, E6′ are higher supersaturated for loeweite and kieserite, respectively, and where the contents of Na^+ and Cl^- simultaneously fit to the nucleation conditions of NaCl. So the coprecipitate paths in the nonequilibrium state are not the same as the cosaturated curves in solubility equilibria.

Stability of Salt-Forming Region in the Nonequilibrium State. Presenting all salt-forming regions in Figures 2 to 5 on the solubility diagram, we obtained the so-called salt-forming diagram.

(1) Figure 6 expresses four one-salt regions (K, L, T, H) and a complex interlaced zone where the univariant curves in solubility diagram become to two-salt overlapped zones (K+L, L+T+V, H+T, L+H, H+K), and the invariant points turn into three-salt overlapped zones (H+T+L+V, H+L+K).

(2) Figure 6 gives some information about the stability of salt-forming regions in the nonequilibrium state. The one-salt region is named the nonequilibrium stable region where the appointed salt solid phase could form whether in primary nucleation or in crystal growth, but other salts could not form in the experimental conditions. On the contrary, the interlaced zones exist and account for about 22.12 % of the total area, which cannot be presented in solubility diagrams or metastable diagrams (because of the phase rule), and could be named as the conditional-region where the forming salt may be one or another or together in the experimental conditions depending on the crystal seed species.

(3) In addition, Figure 6 also shows that the nonequilibrium stable-regions are different from those in solubility diagram. Furthermore, the metastable region, just like the region of "A" appointed in Figure 6, would be stable in the none-quilibrium state.

Salt-Forming Region and Solubility Diagram Region. The salt could stably exist in the equilibrium region and could form in the salt-forming region. Combing these two regions, we obtained an isothermal region for the appointed salt. Figure 7 shows all salt isothermal regions which include four one-salt (K, L, T, H) stable regions, a complex isothermal conditional region of seven two-salt regions (K+H, K+L, L+H, L+V, H+V, T+V, K+T), four three-salt regions (K+L+H, H+L+V, H+T+V), and one four-salt region (H+T+L+V). The isothermal conditional region accounts for 37.6 % of the diagram, where

Table 6. Solid and Liquid Composition in the Isothermal Evaporation Process for the E Series Representative Points

no.	liquid composition (Jänecke index) Na_2^{2+}	SO_4^{2-}	H_2O	pressure KP	solid[a]	no.	liquid composition (Jänecke index) Na_2^{2+}	SO_4^{2-}	H_2O	pressure KP	solid[a]
E01	8.18	100.00	540.00	101.3		E34	8.35	79.79	441.47	18.6	K
E02	8.18	100.00	532.00	29.0	K[b]	E35	10.80	72.53	451.36	18.2	K
E03	8.73	100.00	531.20	28.0	K	E36	12.60	69.07	466.65	18.3	K+L[c]
E04	10.29	100.00	500.38	27.5	K	E37	9.15	63.60	473.52	17.7	L
E05	11.96	100.00	483.52	26.0	K	E41	8.16	50.14	576.25	101.3	
E06	13.67	100.00	463.62	25.6	K	E42	8.16	50.14	531.59	25.5	K[b]
E07	15.21	100.00	460.10	25.0	K+L[c]	E43	10.50	39.83	501.92	23.0	K+H[c]
E11	8.46	89.39	552.00	101.3		E44	6.57	31.86	516.88	22.0	K+H
E12	8.46	89.39	485.30	32.0	K[b]	E45	3.95	22.08	521.85	18.0	K+H
E13	9.19	89.39	483.46	31.0	K	E51	4.42	40.68	630.00	101.3	
E14	12.41	85.92	474.77	31.5	K+L[c]	E52	4.42	40.68	610.00	22.4	K[b]
E15	11.23	80.10	462.93	30.0	L	E53	4.73	39.60	492.95	18.2	K+H[c]
E16	7.21	74.91	492.64	29.6	L	E54	4.27	24.97	509.14	17.7	K+H
E21	5.60	90.00	542.00	101.3		E55	4.15	20.96	511.02	16.7	K+H
E22	5.60	90.00	520.00	32.0	K[b]	E56	2.60	18.94	470.96	15.9	K+H
E23	8.22	85.78	489.31	25.0	K	E61	1.65	29.55	618.82	101.3	
E24	11.42	80.41	546.26	23.8	K	E62	1.65	29.55	508.74	16.9	K[b]
E25	13.22	77.86	562.44	22.9	K	E63	1.52	21.41	508.99	16.6	K
E31	7.39	79.76	562.50	101.3		E64	1.46	18.37	514.34	15.5	K
E32	7.39	79.76	543.00	22.4	K[b]	E65	0.35	12.47	485.57	14.1	K+H[c]
E33	7.48	79.43	480.60	17.7	K	E66	0.05	6.62	420.51	10.1	K+H

[a] K, kieserite ($MgSO_4 \cdot H_2O$); L, loeweite ($Na_2SO_4 \cdot MgSO_4 \cdot 2.5H_2O$); V, vanthofite ($3Na_2SO_4 \cdot MgSO_4$); T, thenardite ($Na_2SO_4$); H, halite (NaCl); T, thenardite (Na_2SO_4), [b] First salt occurring point. [c] Second salt occurring point.

the type of salt formed depends more on the nonthermodynamic conditions, not only the crystal seed, but also the evaporation rate, crystal seed amount, stirring, and so forth.

■ CONCLUSION

Salt-forming behaviors for the quaternary system of Na^+, $Mg^{2+}//Cl^-,SO_4^{2-}-H_2O$ at high temperatures (348.15 K) and at a high evaporation intensity were experimentally studied by the isothermal boiling evaporation method. The salt-forming behavior in some fields in the nonequilibrium state are largely different from the theoretical results on the solubility diagram. The salt-forming regions of the contained salts were determined which largely depart from those in solubility region with different degrees. Meanwhile the salt-forming diagram was composed by the salt-forming regions, and the isothermal diagram made up by the salt-forming region and solubility region was obtained.

As the typical region, the overlapped regions were found and named the conditional region where the type of solid salt precipitated would depend more on the nonthermodynamic conditions, such as crystal seed, evaporation rate, or mixing. It accounts for a large area and is extremely valuable to the industry process.

To learn more about the behaviors of salt forming at high temperatures and at a high evaporation intensity for the complex system, more experiments are still required. Furthermore, the mechanism, thermodynamics, or kinetics models are urgently needed.

■ AUTHOR INFORMATION

Corresponding Author

*Tel.: +8622-60600945; fax: +8622-60600358. E-mail: zhouhuan@tust.edu.cn.

Funding

The authors received financial support from National Natural Science Foundation of China ((No. 20776110, 21176189) and the Nature Science Foundation of Tianjin (No. 11JCZDJC24300).

■ REFERENCES

(1) Voigt, W. Solubility equilibria in multicomponent oceanic salt systems from t = 0 to 200 °C: Model parameterization and databases. *Pure Appl. Chem.* **2001**, *73* (5), 831−844.

(2) Cohen-Adad, R.; Balarew, C.; Tepavitcharova, S. Sea-water solubility phase diagram. Application to an extractive process. *Pure Appl. Chem.* **2002**, *74* (10), 1811−1821.

(3) Kurnakov, N. S.; Nikolaev, V. I. Proceedings of the sector of physico-chemical analysis. *Izv. Sekt. Fiz. Khim. Anal. IONKh, USSR* **1938**, *10*, 333−336.

(4) Jin, Z. M.; Xiao, X. Z. Studies on the meta stable phase equilibrium of Na^+, K^+, $Mg^{2+}//Cl^-$, $SO_4^{2-}-H_2O$ quinary system at 298 K. *Acta Chim. Sin.* **1980**, *38* (4), 313−321.

(5) Jin, Z. M.; Zhou, H. N.; Wang, L. S. Studies on the metastable phase equilibrium of Na^+, K^+, $Mg^{2+}//Cl^-$, $SO_4^{2-}-H_2O$ quinary system at 308 K. *Chem. J. Chin. Univ.* **2001**, *22* (4), 634−638.

(6) Jin, Z. M.; Zhou, H. N.; Wang, L. S. Studies on the metastable phase equilibrium of Na^+, K^+, $Mg^{2+}//Cl^-$, $SO_4^{2-}-H_2O$ quinary system at 288 K. *Chem. J. Chin. Univ.* **2002**, *23* (4), 690−694.

(7) Sang, S. H.; Yin, H. A.; Xing, W. Z. (Solid plus liquid) metastable equilibria in quaternary system (Li_2SO_4 + K_2SO_4 + $Li_2B_4O_7$ + $K_2B_4O_7$ + H_2O) at T = 288 K. *J. Chem. Thermodyn.* **2006**, *38* (2), 173−178.

(8) Sang, S. H.; Yin, H. A.; Zeng, Y. Study on metastable equilibria in quaternary system Li^+, $Na^+//SO_4^{2-}$, $CO_3^{2-}-H_2O$ at 288 K. *Acta Chim. Sin.* **2006**, *64* (22), 2247−2253.

(9) Zeng, Y.; Ling, X. F.; Ni, S. J. Study on the metastable equilibria of the salt lake brine system Li_2SO_4 + Na_2SO_4 + K_2SO_4 + $Li_2B_4O_7$ + $Na_2B_4O_7$ + $K_2B_4O_7$ + H_2O at 288 K. *J. Chem. Eng. Data* **2007**, *52* (1), 164−167.

(10) Zeng., Y.; Meng, Z. Y. Metastable Phase Equilibria for the Quaternary System Na^+ + K^+ + CO_3^{2-} + $B_4O_7^{2-}$ + H_2O at 273.15 K. *J. Chem. Eng. Data* **2010**, *55* (4), 1623−1627.

(11) Deng, T. L.; Wang, S. Q.; Sun, B. Metastable phase equilibrium in the aqueous quaternary system (KCl plus K_2SO_4 + $K_2B_4O_7$ + H_2O) at 308.15 K. *J. Chem. Eng. Data* **2008**, *53* (2), 411−414.

(12) Deng, T. L.; Li, D. C. Solid-liquid metastable equilibria in the quaternary system (NaCl-KCl-$CaCl_2$−H_2O) at 288.15 K. *Fluid Phase Equilib.* **2008**, *269* (1−2), 98−103.

(13) Deng, T. L.; Yu, X.; Li, D. C. Metastable Phase Equilibrium in the Aqueous Ternary System K_2SO_4+ $MgSO_4$+ H_2O at (288.15 and 308.15) K. *J. Solution Chem.* **2009**, *38* (1), 27−34.

(14) Tepavitcharova, S.; Balarew, C.; Rull, F. Raman spectroscopic studies of ion association in the Na^+, Mg^{2+}/Cl^-, SO_4^{2-}//H_2O system. *J. Raman Spectrosc.* **2005**, *36* (9), 891−897.

(15) Tepavitcharova, S.; Balarew, C. D. Crystallisation Kinetics of NaCl, $MgSO_4\cdot H_2O$, $Na_2SO_4\cdot MgSO_4\cdot 4H_2O$ and Na_2SO_4 in the system Na^+,Mg^{2+} /Cl^-,SO_4^{2-}//H_2O at 25 °C. *Freiberg. Forsch. (Naturwiss.)* **2002**, *E3*, 94.

(16) Zhou, H. A method of preparing halite and epsomite with bittern. CN Patent No. 2,008,100,541,98.6, 2008.

(17) Zhou, H.; Cui, S. G.; Sha, Z. L.; Yuan, J. J. Non-equilibrium behavior of salt-forming in boiling evaporation process for the system of $MgSO_4$-Na_2SO_4−H_2O at 373 K. *Acta Chim. Sin.* **2008**, *66* (12), 1483−1489.

(18) Zhou, H.; Cui, S. G.; Sha, Z. L.; Yuan, J. J. Non-equilibrium behavior of salt-forming in boiling evaporation process for the system of $MgSO_4$-K_2SO_4−H_2O at 348 K. *Chem. J. Chin. Univ.* **2008**, *29* (10), 2049−2054.

(19) Zhou, H.; Chen, Y. D.; Zhang, Q. D. Non-equilibrium State Salt-forming Phase Diagram Applica-tion to the Utilization of Bittern Resource in high Efficiency. *Chin. J. Chem. Eng.* **2010**, *18* (4), 635−641.

(20) Howard, S. *Solubilities of Inorganic and Organic Compounds*; Pergamon Press: New York, 1979.